

ANALYSIS OF MODEL OUTPUT IN THE SIMULATION OF A WHEELCHAIR-OCCUPANT SYSTEM SUBJECTED TO VIBRATION

PONGTEP WEERAPONG^{1,2,*}, KOTARO HASHIKURA³, MD ABDUS SAMAD KAMAL³
IWANORI MURAKAMI³ AND KOU YAMADA³

¹Department of Production Technology
Faculty of Industrial Technology
Nakhon Si Thammarat Rajabhat University
M4 Tha-Ngow Subdistrict, Maung District, Nakhon Si Thammarat 80280, Thailand

*Corresponding author: pongtap_wee@nstru.ac.th

²Graduate School of Science and Technology
³Division of Mechanical Science and Technology
Gunma University

1-5-1 Tenjincho, Kiryu 376-8515, Japan
{ t202b007; k-hashikura; maskamal; murakami; yamada }@gunma-u.ac.jp

Received September 2022; accepted December 2022

ABSTRACT. *This study seeks to evaluate the accuracy of the output from a wheelchair-occupant simulation model in comparison with real-world experimental results from industry literature. Different model setups, in which the wheelchair's occupant is supported on three types of seat cushion, are formulated with the model being subjected to low-frequency vibration waves arising from the interaction between wheelchair tires and ground profile. The model's outputs, i.e., the predictions of comfort evaluation in terms of seat-to-head (STH) transmissibility, driving-point mechanical (DPM) impedance, and apparent (AP) mass with goodness-of-fit values obtained from our 11-DOF simulation model, are seen to fall far below the target values obtained in actual reported experiments. This may be remedied in future work by using suitable target values of dynamic stiffness and damping constant that would yield better seat responses applicable to increasing human ride comfort.*

Keywords: Mathematical model, Wheelchair, 11-DOF, Wheelchair-occupant system

1. Introduction. Wheelchair riders are exposed to vibration arising from wheelchair operation and thus are vulnerable to physical discomfort which may lead to severe, chronic illnesses [1]. Good wheelchair engineering can help to reduce vibration and many design approaches have been proposed [2, 3, 4]. One of the most economical and accessible design options is in modifying the seat cushion [5]. The decision on which seat cushion to use can be made from experiments with actual cushion products, or through computer simulation involving the potential materials [6, 7]. Garcia-Mendez et al. [5] tested seven types of seat cushion in order to study the vibration transmissibility of the seat assembly. The results were corroborated by Weerapong et al. [8, 9] who employed a simulation model with nine degrees of freedom (9-DOF) to study the vibration on the wheelchair occupant seated on selected types of seat cushion. Such approaches have been found to be effective in reducing shocks to the occupant's body over the vibration frequency range of 0.5 to 20 [Hz] [10, 11]. This study is an effort to extend the author's previously 9-DOF model to 11-DOF [12, 13]. The additional dimensions are needed in order to isolate the model's wheels from its suspension mechanism. The isolated dimensions would enable direct analyses of

the forces acting on the seat cushion – an improvement that was lacking in the previous 9-DOF model.

In this paper, we explain the approach we employed to predict the dynamic behavior [11, 14] of the wheelchair-occupant model. Simulations were carried out over a reported frequency domain in order to compare the simulated wheelchair ride quality against the results obtained from real-world experiments [12] wherein the human subject’s body was exposed to vertical vibration [11]. Our results were found to correlate well with those of the reported experiments. They also suggest the possibility of increasing the human ride comfort through using suitable target values of dynamic stiffness and damping constant that should yield better wheelchair seat responses. This paper is organized as follows. In Section 2, we analyze the wheelchair and occupant segments regarding properties of human tissue, spring and damper, and define the force vectors upon the masses in the free body diagrams. In Section 3, the model’s EOMs are transformed, using Fourier transformation and Euler’s formula, into matrices containing frequency response functions. Section 4 deals with model evaluation and validation, and application of its responses to obtain the values of seat-to-head (STH) transmissibility, driving-point mechanical (DPM) impedance and apparent (AP) mass. Section 5 gives some concluding remarks.

2. Analysis of Lumped Mechanical System. Construction of the wheelchair-occupant system is outlined in Figure 1. The 4-DOF wheelchair is represented by four blocks: 1) the seat, padded with a cushion of negligible mass; 2) chair frame; 3) front tires; and 4) rear tires – these are denoted by m_8, m_9, m_{10} and m_{11} . The occupant, as a 7-DOF frame emulating the work of Liang and Chiang [11] with an idealized sitting human anatomy, has its parts isolated at the joints where relative movements are allowed, and the parts considered as lumped masses. The seven blocks, comprising head (m_1), back (m_2), torso (m_3), thorax (m_4), diaphragm (m_5), abdomen (m_6), and pelvis (m_7), are connected by

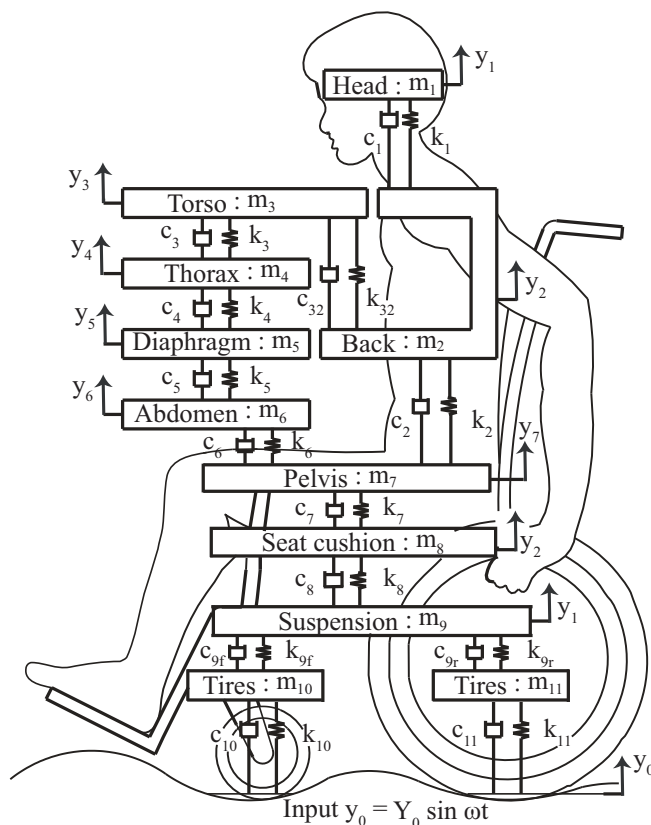


FIGURE 1. Eleven lumped mass model of wheelchair-occupant system

TABLE 1. Parameter values of occupant model [11]

Mass [M] (kg)	Damping constant [C] (N/m/sec)	Spring constant [K] (N/m)
$m_7 = 27.7$	$c_7 = 378$	$k_7 = 25500$
$m_6 = 6.02$	$c_6 = 298$	$k_6 = 894.1$
$m_5 = 0.46$	$c_5 = 298$	$k_5 = 894.1$
$m_4 = 1.38$	$c_4 = 298$	$k_4 = 894.1$
$m_3 = 33.33$	$c_3 = 298$	$k_3 = 894.1$
	$c_{32} = 3651$	$k_{32} = 53640$
$m_2 = 6.94$	$c_2 = 3651$	$k_2 = 53640$
$m_1 = 5.5$	$c_1 = 3651$	$k_1 = 53640$

springs and dampers, representing the resilient characteristics of the connective tissues between the components. The parameter values of such human tissues, obtained from various studies of anatomical subsystems, are listed in Table 1.

The wheelchair is modeled as a typical manual device which is employed for travels on typical urban traffic surfaces. The occupant body is set in a seated posture with its lower segments supported by the seat cushion, and the upper segments unsupported by a back-rest. The input vibrations are limited to those coming from the sinusoidal functions of the springs and dampers on the wheelchair tires and emanating through the seat cushion to the occupant’s body. Amplitude of the input wave is set at 0.005 m. The real-world vibrations through the wheelchair foot support are ignored in the simulation as they are negligibly small in magnitude and would affect only the trunk. Figure 1 diagrams the wheelchair and occupant in cross-section having eleven blocks of mass denoted by m_i ($i = 1, \dots, 11$). The blocks are connected in pairs with a spring and a dashpot whose stiffness and damping coefficients are denoted by k_i and c_i . These k_i and c_i values have been obtained from previously published experimental results. They are listed in Tables 1 and 2.

TABLE 2. Parameter values of manual wheelchair [5, 15]

Mass [M] (kg)	Damping constant [C] (N/m/sec)	Spring constant [K] (N/m)
$m_{11} = 1.6$	$c_{11} = 500$	$k_{11} = 6000$
$m_{10} = 1.0$	$c_{10} = 500$	$k_{10} = 60000$
$m_9 = 15$	$c_{9f} = 700$	$k_{9f} = 13400$
	$c_{9r} = 700$	$k_{9r} = 74600$
$m_8 = 1.5$	$c_{8a} = 834$	$k_{8a} = 94220$
	$c_{8b} = 571$	$k_{8b} = 39970$
	$c_{8c} = 1507$	$k_{8c} = 174900$
Input magnitude vibration, $y_0 = 5.0$ mm.		

f and r denote the parameter values for suspension: f , for front; r , for rear. a , b and c denote the parameter values of the cushion types: a for air-based Roho High Profile; b for gel-based Jay J2 Deep Contour; and c for foam-based Zoombang Protective Gear with Foam.

3. Mathematical Model and Measurements. In this section, we explain the model’s EOMs which, after manipulation with Fourier transformation and Euler’s formula, are arranged as matrices containing frequency response functions.

The following assumptions are made regarding the 11-DOF lumped-mass model.

- 1) Motions are confined in the vertical direction.
- 2) The ground profile is of a sinusoidal shape having 5 mm (0.005 m) amplitude.
- 3) Spring and damper characteristics are linear.

Our EOMs are based on the diagram in Figure 1. An EOM contains several terms, including a mass, its inertia, and forces acting on it by the springs and dashpots. The terms $y_0(t)$ and $\dot{y}_0(t)$ signify the displacements and velocities of a mass occurring upon excitation. Full EOMs for the system in Figure 1 are shown below.

3.1. Derivation of EOMs in matrix form. These EOMs can be expressed in matrix form as

$$[M]\{\ddot{y}(t)\} + [C]\{\dot{y}(t)\} + [K]\{y(t)\} = \{F\} \sin \omega t, \quad (1)$$

where $[M]$, $[K]$, and $[C]$ represent 11×11 matrices denoting respectively the mass, stiffness and damping matrices. $\{y(t)\}$, $\{\dot{y}(t)\}$, and $\{\ddot{y}(t)\}$ represent displacement, velocity and acceleration vectors of response, respectively and ω represents the excitation frequency. Elements of these matrices were obtained from the EOMs given from Equations (2) to (12). With the mass matrix, its elements are zero except those on its diagonal. $\{F\}$ is an 11×1 force matrix whose elements are zero except those on the 10th and 11th rows which represent the sinusoidal forces given in Equations (11) and (12).

3.2. The equations of motion for lumped masses. EOMs are summarized as

1. The head

$$m_1 \ddot{y}_1 + c_1(\dot{y}_1 - \dot{y}_2) + k_1(y_1 - y_2) = 0, \quad (2)$$

2. The back

$$m_2 \ddot{y}_2 + c_1(\dot{y}_2 - \dot{y}_1) + c_{32}(\dot{y}_2 - \dot{y}_3) + c_2(\dot{y}_2 - \dot{y}_3) + k_1(y_2 - y_1) + k_2(y_2 - y_3) + k_{32}(y_2 - y_3) = 0, \quad (3)$$

3. The torso

$$m_3 \ddot{y}_3 + c_{32}(\dot{y}_3 - \dot{y}_2) + c_3(\dot{y}_3 - \dot{y}_4) + k_{32}(y_3 - y_2) + k_3(y_3 - y_4) = 0, \quad (4)$$

4. The thorax

$$m_4 \ddot{y}_4 + c_3(\dot{y}_4 - \dot{y}_3) + c_4(\dot{y}_4 - \dot{y}_5) + k_3(y_4 - y_3) + k_4(y_4 - y_5) = 0, \quad (5)$$

5. The diaphragm

$$m_5 \ddot{y}_5 + c_4(\dot{y}_5 - \dot{y}_4) + c_5(\dot{y}_5 - \dot{y}_6) + k_4(y_5 - y_4) + k_5(y_5 - y_6) = 0, \quad (6)$$

6. The abdomen

$$m_6 \ddot{y}_6 + c_5(\dot{y}_6 - \dot{y}_5) + c_6(\dot{y}_6 - \dot{y}_7) + k_5(y_6 - y_5) + k_6(y_6 - y_7) = 0, \quad (7)$$

7. The pelvis

$$m_7 \ddot{y}_7 + c_6(\dot{y}_7 - \dot{y}_6) + c_7(\dot{y}_7 - \dot{y}_2) + c_2(\dot{y}_7 - \dot{y}_2) + k_6(y_7 - y_6) + k_7(y_7 - y_2) + k_2(y_7 - y_2) = 0, \quad (8)$$

8. The seat cushion

$$m_8 \ddot{y}_8 + c_7(\dot{y}_8 - \dot{y}_7) + c_8(\dot{y}_8 - \dot{y}_9) + k_7(y_8 - y_7) + k_8(y_8 - y_9) = 0, \quad (9)$$

9. The suspension

$$m_9 \ddot{y}_9 + c_8(\dot{y}_9 - \dot{y}_8) + c_{9f}(\dot{y}_9 - \dot{y}_{10}) + c_{9r}(\dot{y}_9 - \dot{y}_{11}) + k_{9r}(y_9 - y_{11}) + k_{9f}(y_9 - y_{10}) + k_8(y_9 - y_8) = 0, \quad (10)$$

10. The front tires

$$m_{10} \ddot{y}_{10} + c_{9f}(\dot{y}_{10} - \dot{y}_9) + c_{10}(\dot{y}_{10} - \dot{y}_0) + k_{9f}(y_{10} - y_9) + k_{10}(y_{10} - y_0) = c_{10}y_0\omega\cos\omega t + k_{10}y_0\sin\omega t \quad (11)$$

and

11. The rear tires

$$m_{11} \ddot{y}_{11} + c_{9r}(\dot{y}_{11} - \dot{y}_9) + c_{11}(\dot{y}_{11} - \dot{y}_0) + k_{9r}(y_{11} - y_9) + k_{11}(y_{11} - y_0) = c_{11}y_0\omega\cos\omega t + k_{11}y_0\sin\omega t. \quad (12)$$

3.3. Matrix form of the complex Fourier transformation. Fourier transformation is applied with Euler’s formula $e^{i\omega t} = \cos \omega t + i \sin \omega t$ and the transforms then brought to substitute into (1) of the steady-state response. The derivatives of equation of excitation from the base state and response are given by $\{y_0(t)\} = \{Y_0\}e^{i\omega t}$ and $\{y(t)\} = \{Y\}e^{i\omega t}$, respectively. By substituting $y_0(t)$, $\dot{y}_0(t)$, $y(t)$, $\dot{y}(t)$, $\ddot{y}(t)$ of exponential function vectors of the excitation and response into Equation (1), we obtain the matrix equation for the multiple degree of freedom (MDOF) system as shown by

$$[-\omega^2[M] + i\omega[C] + [K]] \{Y\}e^{i\omega t} = \{F\}e^{i\omega t}. \tag{13}$$

3.4. Solving for displacement in the complex function. EOMs of the 11-DOF system are substituted into the complex terms in the transfer function (expressed in hertz) in (13). Further manipulation of this equation enables us to eliminate the time-dependent part, thereby yielding

$$\{Y_k(i\omega)\} = \frac{\{F_k(i\omega)\}}{[-\omega^2[M] + i\omega[C] + [K]]}, \tag{14}$$

where $\{Y_k(i\omega)\}$ and $\{F_k(i\omega)\}$ are the corresponding complex Fourier transform vectors of displacement and excitation force, respectively; while $[M] = m_{kl}$, $[C] = c_{kl}$, and $[K] = k_{kl}$; ($k, l = 1, \dots, 11$), are the mass, damper and stiffness matrices of the body and wheelchair segments; and ω , the excitation frequency.

Upon setting the input excitation forces to zero – or $F_k(i\omega)$, ($k = 1, \dots, 9$) = 0 – only two excitation forces remained, namely the forces at the front and rear tyres, or $F_{10}(i\omega) = (i\omega c_{10} + k_{10})Y_0$ and $F_{11}(i\omega) = (i\omega c_{11} + k_{11})Y_0$. The rest of the internal forces became zero. Substituting these values into Equation (14), we obtain the displacement values of each DOF of the body and wheelchair segments as

$$\{Y_k(i\omega)\} = \frac{((k_{10} + k_{11}) + i\omega(c_{10} + c_{11}))Y_0(i\omega)}{(-\omega^2 m_{kl} + k_{kl} + i\omega c_{kl})}. \tag{15}$$

Next, we examine (14). The $[-\omega^2[M] + i\omega[C] + [K]]$ term therein is impedance matrix for assessing mechanical responses from the human and vehicle frames, and it may be expressed in transfer function matrices as shown below. $\{Y_k(i\omega)\}$ and $\{F_k(i\omega)\}$ are the corresponding complex Fourier transform vectors of $Y_k(i\omega)$ and $F_k(i\omega)$, respectively and ω , the excitation frequency. Upon substitution in (14), we have

$$\frac{Y_k(i\omega)}{F_k(i\omega)} = \frac{1}{-\omega^2 m_{kl} + i\omega c_{kl} + k_{kl}} = H_{kl}(i\omega), \quad (k, l = 1, \dots, 11), \tag{16}$$

where $H_{kl}(i\omega)$ is response at mass of k per unit force excitation at l . The $[-\omega^2[M] + i\omega[C] + [K]]$ portion has been generated by the equations of mass, damping and stiffness matrices. Its inverse, as shown in (17), became the transfer function which is $[H_{kl}(i\omega)]$. This gave us the set of matrix equations as

$$= \begin{bmatrix} H_{11}(i\omega) & H_{12}(i\omega) & H_{13}(i\omega) & \dots & H_{1(11)}(i\omega) \\ H_{21}(i\omega) & H_{22}(i\omega) & H_{23}(i\omega) & \dots & H_{2(11)}(i\omega) \\ H_{31}(i\omega) & H_{32}(i\omega) & H_{33}(i\omega) & \dots & H_{3(11)}(i\omega) \\ \vdots & \vdots & \vdots & \ddots & \vdots \\ H_{(11)1}(i\omega) & H_{(11)2}(i\omega) & H_{(11)3}(i\omega) & \dots & H_{(11)(11)}(i\omega) \end{bmatrix} \begin{Bmatrix} Y_1(i\omega) \\ Y_2(i\omega) \\ Y_3(i\omega) \\ \vdots \\ Y_{11}(i\omega) \end{Bmatrix} = \begin{Bmatrix} F_1(i\omega) \\ F_2(i\omega) \\ F_3(i\omega) \\ \vdots \\ F_{11}(i\omega) \end{Bmatrix}^{-1}. \tag{17}$$

As laid out above, $[H_{kl}(i\omega)]$ ($k, l = 1, \dots, 11$) is an 11 by 11 matrix of transfer functions with 121 possible contributions. By using $Y_k(i\omega)$ ($k = 1, \dots, 11$) and setting the input force vectors $F_k(i\omega) = 0$ ($k = 1, \dots, 9$), we obtain the displacement values of each DOF of the body segments and wheelchair components from

$$\begin{cases} Y_1(i\omega) = H_{1(10)}(i\omega)F_{10}(i\omega) + H_{1(11)}(i\omega)F_{11}(i\omega), \\ Y_2(i\omega) = H_{2(10)}(i\omega)F_{10}(i\omega) + H_{2(11)}(i\omega)F_{11}(i\omega), \\ Y_3(i\omega) = H_{3(10)}(i\omega)F_{10}(i\omega) + H_{3(11)}(i\omega)F_{11}(i\omega), \\ \vdots \\ Y_{11}(i\omega) = H_{11(10)}(i\omega)F_{10}(i\omega) + H_{11(11)}(i\omega)F_{11}(i\omega). \end{cases} \quad (18)$$

3.5. Approaches for solving the EOMs in multi-degree of freedom. The responses from the model are evaluated against published results of experimental measurement of whole-body vibration which are adopted as our test datum. For this study, three key attributes of the responses are assessed: STH, DPM impedance and AP mass, as explained below. The proximity of the model results to the test datum is expressed as goodness-of-fit.

3.5.1. Transmissibility. Transmissibility is the ratio of the displacement response at a point on the occupant body to the displacement at the wheelchair seat; or the ratio of output response versus input excitation – and typically called displacement ratio. For example, for STH transmissibility, it can be expressed using the above definition as

$$STH = \frac{|Y_1(i\omega)|}{|Y_0(i\omega)|}, \quad (19)$$

where $|Y_1(i\omega)|$ represents the magnitudes of displacement response from the occupant’s head (m_1) and $|Y_0(i\omega)|$ the magnitudes of input excitation on the wheelchair seat.

3.5.2. DPM impedance. DPM impedance is the complex ratio of the force applied to an element at frequency ω , to the resulting vibration velocity of the impacted element at that frequency. This function is defined as the ratio of the driving force (summation of spring and damping forces between pelvis and seat in Patil’s model) to the driving-point velocity (input velocity to the seat). Accordingly, DPM impedance can be expressed as

$$DPM = \frac{|(k_7 + i\omega c_7)(Y_8(i\omega) - Y_7(i\omega))|}{|i\omega Y_8(i\omega)|}, \quad (20)$$

where $Y_7(i\omega)$ is the magnitude of displacement response exhibited by the occupant’s pelvis (m_7) and $Y_8(i\omega)$, similar magnitude measured at the wheelchair seat (m_8).

3.5.3. AP mass. AP mass functions as the human body. The force required to accelerate the buttocks of the occupant, through which the vibration waves are transmitted, is a complex function of frequency, which can be expressed in terms of $DPM(i\omega)^{-1}$ as

$$AP = \frac{|(k_7 + i\omega c_7)(Y_8(i\omega) - Y_7(i\omega))|}{|(i\omega)^2 Y_8(i\omega)|}. \quad (21)$$

3.5.4. Goodness-of-fit. Goodness-of-fit is a statistical test to check the proximity of a response data point to the value of an established datum. In our case, the model simulation results are compared against published experimental values. Goodness-of-it is expressed as the ratio of the root-mean-square error of the test results to the mean value of published data. Accordingly, the goodness-of-fit, denoted by ϵ [11] is written as

$$\epsilon = 1 - \frac{\sqrt{\frac{\sum_{m=1}^N (\tau_m - \tau_c)^2}{N-2}}}{\frac{\sum_{m=1}^N \tau_m}{N}}, \quad (22)$$

where τ_m is the test datum, τ_c the calculated result from each model, and N , the number of test data points used in the comparison. The value of ϵ indicates the quality of data fit. As ϵ approaches 1, the predicted results approach a perfect fit with the published data.

4. Results and Discussions. In this section, we explain the results of our simulations.

4.1. Validation of the 11-DOF model with different cushion types. The thorax-to-pelvis displacement ratios given out by our model are shown in Figure 2 as a function of input frequency. From the figure, we see that the first peak value occurs at frequency of approximately 3 [Hz], and the lowest values at the range of 0.5 to 11 [Hz].

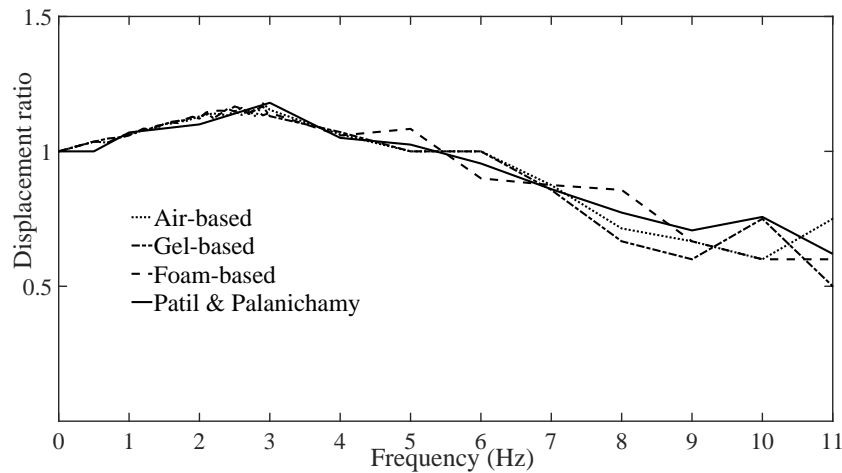


FIGURE 2. Thorax-to-pelvis displacement ratios obtained from tests on air-, gel-, and foam-based cushions

Superimposed thereon is the experimental curve derived by Patil and Palanichamy [16], from tests using sinusoidal inputs. Since good agreement can be seen between our results and those of corresponding experiment, we may conclude that our composite model is of acceptable quality. Tables 1 and 2 list the values of parameters for stiffness and damping applicable to the tested air-, gel- and foam-based seat cushions.

4.2. Biodynamic evaluation of the wheelchair and occupant model. Over the years, the biodynamic responses of the seated human figure exposed to vertical vibration have been widely investigated in terms of seat-to-head (or STH) transmissibility, DPM impedance and AP mass. Several mathematical models have been fashioned by different investigators with varying degrees of complexity. Also, volumes of data have been generated to characterize these response functions under varying experimental conditions. For brevity purposes, only those data that have been compiled through the use of mathematical models under a well-defined range of assumptions are listed in this study.

4.3. Comparisons of human ride comfort for the predicted goodness-of-fit. Figures 3, 4 and 5 show the resulting transmissibility values associated with the seat-to-head segment, DPM impedance and AP mass. The solid line, together with its upper and lower limits running across the figures, defines the target values of comfort and health safety, i.e., a boundary of transmissibility below which offending vibrations should be confined. These target values are outcomes of tests by Liang and Chiang [11] which yield the apexes of transmissibility at 5.1 [Hz] when comparison is made with different seat cushions on standard wheelchairs. The goodness-of-fit for the model runs was calculated using Equation (22) above, and the results were tabulated in Table 3. At the peak of STH transmissibility from the head mass m_1 , it is found that the gel-based type has the highest response

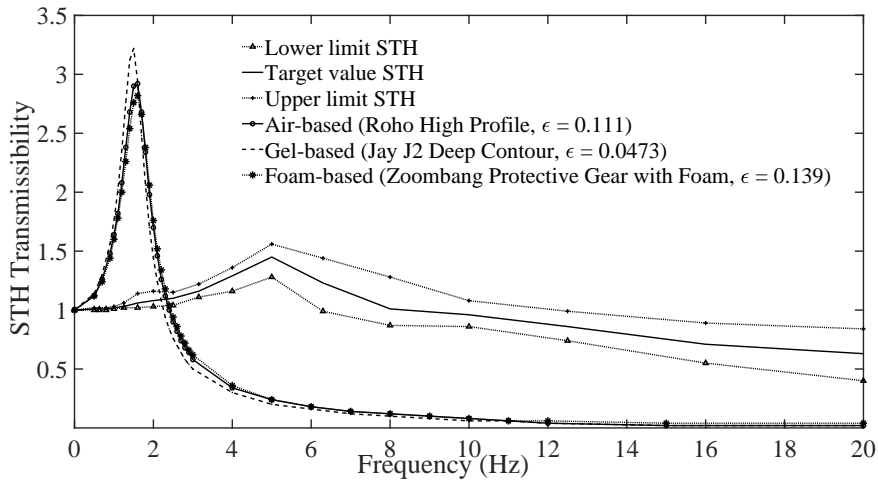


FIGURE 3. Comparison of STH transmissibility in tests with air-, gel-, and foam-based cushions

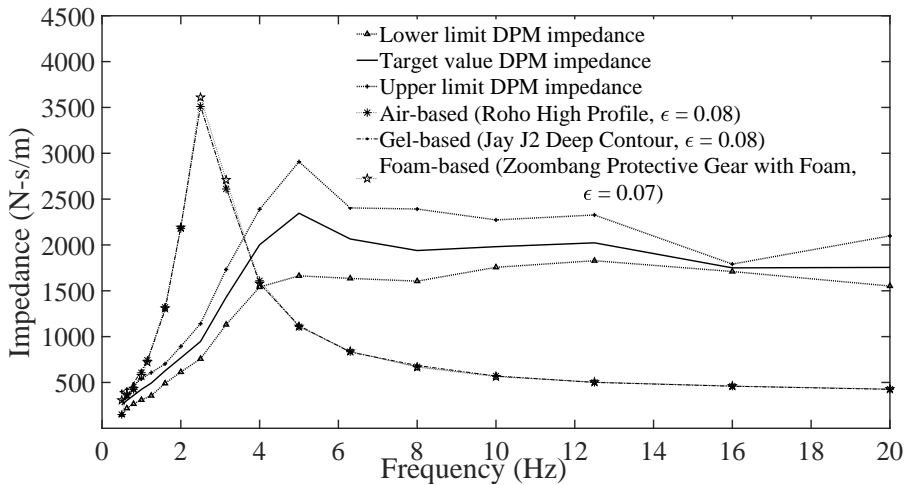


FIGURE 4. Comparison of driving-point mechanical impedance in tests with air-, gel-, and foam-based cushions

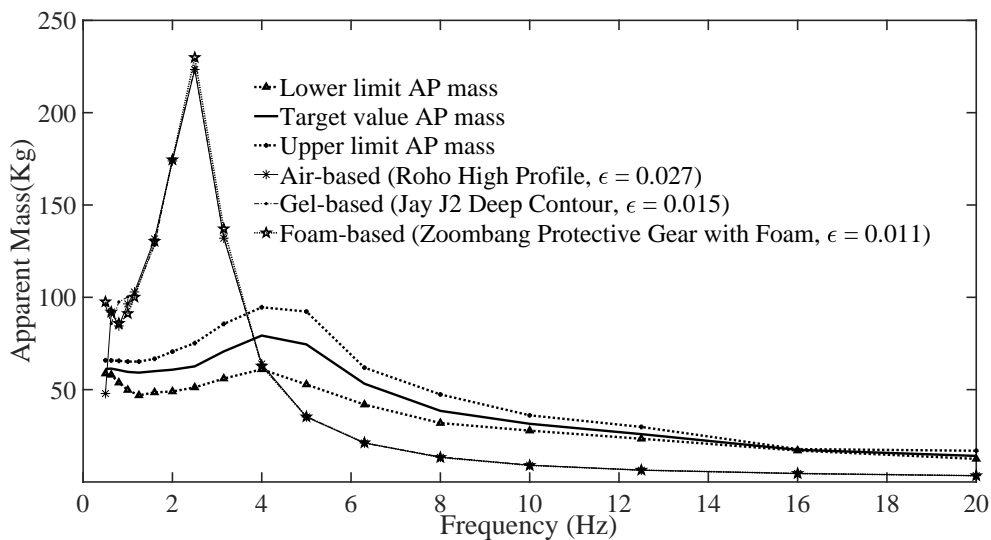


FIGURE 5. Comparison of apparent mass in tests with air-, gel-, and foam-based cushions

amplitude at frequency 1.5 [Hz]; while the foam-based the lowest at 1.6 [Hz]. When stiffness constant was raised, the resultant peak would occur at a lower value – given that resonance frequency is inversely proportional to k . At higher frequency ranges the resonance frequency is no longer dependent on stiffness constant. This would make the peak of the graph become flatter and flatter. At the excitation frequency range employed in this study, the amplitudes of transmissibility appeared to behave in the manner explained. Therefore, we see that the resonance frequency can be controlled by damping. Figure 4 shows the results of DPM impedance in tests with the cushion types. At the resonance frequency of 2.5 [Hz], the respective impedances observed are 3,510, 3,520 and 3,610 [Ns/m]. The impedance is seen to increase with frequency from 0 to 2.5 [Hz], and thereafter decrease as frequency continues to rise from about 2.6 to 20 [Hz]. This indicates that DPM impedance reacts to excitation frequency much like a physical mass. Figure 5 shows the values of AP mass for air-, gel- and foam-based cushions also exhibiting a similar behavior, i.e., reaching a resonance peak at 2.5 [Hz] with AP masses of 223.9, 224.1 and 229.8 [kg], respectively. This indicates that the vibration on wheelchair and seat cushion has an influence on the biodynamic response as predicted, with the foam-based AP mass having the highest value.

The goodness-of-fit calculations for STH transmissibility, DPM impedance and AP mass for the three cushion types are tabulated in Table 3 below. Table 3 shows that the model puts out disappointingly low predictions for STH transmissibility, DPM impedance, as well as poor results in the case of AP mass, when compared against actual experimental values (see Figure 5).

TABLE 3. Goodness-of-fit (ϵ) at resonance frequency (f [Hz]) among air-gel- and foam-based results from model runs

Cushion	STH		DPM		AP mass	
	f	ϵ	f	ϵ	f	ϵ
Air-based	1.6	0.111	2.5	0.08	2.5	0.027
Gel-based	1.5	0.047	2.5	0.08	2.5	0.015
Foam-based	1.6	0.139	2.5	0.07	2.5	0.011

5. Conclusion. Our predictions of comfort level in terms of STH transmissibility, DPM impedance, and AP mass through the use of goodness-of-fit tests with an 11-DOF model are all found to fall far below the target values from actual experiments reported in industry literature. With the three cushion types tested, their vibration effects obtained from the tests were unvarying, having only slight differences in goodness-of-fit values. Such slight differences alone are not significant enough for us to rate the materials. For future work, we shall design suitable values of dynamic stiffness and damping constant that should yield better seat response applicable to increasing human ride comfort.

Acknowledgment. This paper is supported by JSPS KAKENHI Grant Number JP21K03930 and the Royal Thai Government Scholarship.

REFERENCES

[1] M. L. Toro-Hernandez, L. Alvarez, M. C. Vargas-Chaparro and M. Goldberg, Final year students’ knowledge on basic manual wheelchair provision: The state of occupational therapy programs in Colombia, *Occupational Therapy International*, vol.2020, pp.1-8, 3025456, 2020.

[2] O. Lariviere, D. Chadeaux, C. Sauret and P. Thoreux, Vibration transmission during manual wheelchair propulsion: A systematic review, *Vibration*, vol.4, pp.444-481, 2021.

[3] Y. Garcia-Mendez, J. L. Pearlman, M. L. Boninger and R. A. Cooper, Health risks of vibration exposure to wheelchair users in the community, *The Journal of Spinal Cord Medicine*, vol.36, pp.365-375, 2013.

- [4] M. J. Griffin, Discomfort from feeling vehicle vibration, *Vehicle System Dynamics*, vol.45, pp.679-688, 2007.
- [5] Y. Garcia-Mendez, J. L. Pearlman, R. A. Cooper and M. L. Boninger, Dynamic stiffness and transmissibility of commercially available wheelchair cushions using a laboratory test method, *Journal of Rehabilitation Research & Development*, vol.49, no.1, pp.7-22, 2012.
- [6] T. Waga, S. Ura, M. Nagamori, H. Uchiyama and A. Shionoya, Influence of material on wheelchair vibrations, *The 13th Conference of the International Sports Engineering Association*, pp.1-6, 2020.
- [7] F. Chénier and R. Aissaoui, Effect of wheelchair frame material on users' mechanical work and transmitted vibration, *BioMed Research International*, vol.2014, pp.1-12, 609369, 2014.
- [8] P. Weerapong, K. Hashikura, M. A. S. Kamal and K. Yamada, A model for the response of an occupant and wheelchair system subjected to vertical vibrations, *International Journal of Innovative Computing, Information and Control*, vol.17, no.6, pp.1823-1841, 2021.
- [9] P. Weerapong, K. Hashikura, M. A. S. Kamal and K. Yamada, A biodynamic model of wheelchair with changeable seat cushions subjected to vertical vibrations, *ICIC Express Letters*, vol.16, no.1, pp.33-41, 2022.
- [10] S. N. W. Vorrink, L. H. V. Van der Woude, A. Messenberg, P. A. Cripton, B. Hughes and B. J. Sawatzky, Comparison of wheelchair wheels in terms of vibration and spasticity in people with spinal cord injury, *Journal of Rehabilitation Research & Development*, vol.45, pp.1269-1280, 2008.
- [11] C. C. Liang and C. F. Chiang, A study on biodynamic models of seated human subjects exposed to vertical vibration, *International Journal of Industrial Ergonomics*, vol.36, pp.869-890, 2006.
- [12] P. Weerapong, K. Hashikura, M. A. S. Kamal and K. Yamada, A numerical study of model output for whole-body vibration on varying wheelchair cushions, *Proc. of the 7th International Conference on Business and Industrial Research*, 2022.
- [13] P. Weerapong, K. Hashikura, M. A. S. Kamal, I. Murakami and K. Yamada, Simulated response analysis: Modelling a wheelchair-occupant system subjected to vibration, *International Journal of Innovative Computing, Information and Control*, vol.19, no.2, pp.307-323, 2023.
- [14] J. Gao, A. Sha, Y. Huang, L. Hu, Z. Tong and W. Jiang, Evaluating the cycling comfort on urban roads based on cyclists' perception of vibration, *Journal of Cleaner Production*, vol.192, pp.531-541, 2018.
- [15] M. F. Hikmawan and A. S. Nugraha, Analysis of electric wheelchair passenger comfort with a half car model approach, *2016 International Conference on Sustainable Energy Engineering and Application (ICSEEA)*, pp.76-80, 2016.
- [16] M. K. Patil and M. S. Palanichamy, A mathematical model of tractor-occupant system with a new seat suspension for minimization of vibration response, *Applied Mathematical Modelling*, vol.12, pp.63-71, 1988.